

Joint Beamforming for RIS-Assisted Integrated Sensing and Communication Systems

Yongqing Xu, *Graduate Student Member, IEEE*, Yong Li, *Member, IEEE*,
J. Andrew Zhang, *Senior Member, IEEE*, and Marco Di Renzo, *Fellow, IEEE*

Abstract

Integrated sensing and communications (ISAC) is emerging as a critical technique for next-generation communication systems. Reconfigurable intelligent surface (RIS) can simultaneously enhance the performance of communication and sensing by introducing new degrees-of-freedom for beamforming in ISAC systems. This paper proposes two optimization techniques for joint beamforming in RIS-assisted ISAC systems. We first aim to maximize the radar mutual information (MI) by imposing constraints on communication rate, transmit power, and unit modulus reflection coefficients at the RIS. An alternating optimization (AO) algorithm based on the semidefinite relaxation (SDR) method is proposed to solve the optimization problem by introducing a convergence-accelerating method. To achieve lower computational complexity and better reliability, we then formulate a new optimization problem for maximizing the weighted ISAC performance metrics under fewer constraints. An AO algorithm based on the Riemannian gradient (RG) method is proposed to solve this problem. This is achieved by reformulating the transmit and RIS beamforming on the complex hypersphere manifold and complex circle manifold, respectively. Numerical results show that the proposed algorithms can enhance the radar MI and the weighted communication rate simultaneously. The AO algorithm based on RG exhibits better performance than the SDR-based method.

I. INTRODUCTION

Many emerging applications for future networks, such as vehicle-to-everything and smart homes, require high-quality communication performance and demand accurate sensing capabilities [1], [2]. The communication and sensing functionality can be simultaneously realized in a unified platform due to their similar hardware architecture and signal processing algorithms.

Y. Xu and Y. Li are with the Key Laboratory of Universal Wireless Communications, Beijing University of Posts and Telecommunications, Beijing 100876, China. Email: {xuyongqing; liyong}@bupt.edu.cn.

J. Andrew Zhang is with the Global Big Data Technologies Centre (GBDTC) and the School of Electrical and Data Engineering, The University of Technology Sydney (UTS), Sydney, NSW 2007, Australia. Email: Andrew.Zhang@uts.edu.au.

M. Di Renzo is with Université Paris-Saclay, CNRS, CentraleSupélec, Laboratoire des Signaux et Systèmes, 3 Rue Joliot-Curie, 91192 Gif-sur-Yvette, France. (marco.di-renzo@universite-paris-saclay.fr).

Motivated by these considerations, research on integrated sensing and communication (ISAC) is currently underway to empower next-generation communication systems with sensing capabilities. ISAC can realize dynamic spectrum sharing between sensing and communication and achieve an harmonious co-existence between radar and communication systems [3].

According to [4], [5], ISAC can be realized via beamforming. The authors of [6] design the radar beamforming to project the radar signals onto the null space of the interference channel for radar/communication coexistence. A robust multiple-input multiple-output (MIMO) beamforming scheme is also proposed in [7] for ensuring vehicular communication and radar coexistence under imperfect channel state information (CSI). Moreover, the authors of [8] propose to use efficient manifold algorithms to solve the ISAC beamforming problem and analyze the performance offered by them. The beamforming schemes in [9], [10] are based on orthogonal frequency-division multiplexing (OFDM). The authors of [9] design the transmit/receive radar beampatterns and the receive communication beampattern to maximize the Kullback-Leibler divergence (KLD) and to satisfy the signal-to-noise-plus-interference constraints of the communication users. The authors of [10] propose a novel adaptive OFDM waveform to maximize the radar mutual information (MI) and the communication rate. Additionally, the authors of [11] design a frequency-hopping waveform and develop accurate methods to estimate the timing offset and the channel based on the designed waveform. However, the degrees-of-freedom of ISAC beamforming are limited due to the joint design for communication and sensing, since the beamforming are required to satisfy the communication and sensing performance metrics simultaneously.

Reconfigurable intelligent surface (RIS) is a planar surface composed of a large number of low-cost and nearly passive reconfigurable elements, which can be dynamically controlled to induce appropriate amplitude and phase shifts to the incident signals [12]–[15]. With the help of RISs, the degrees-of-freedom for ISAC beamforming increase, and the signal coverage of RIS-assisted ISAC systems is enhanced. Many papers have investigated how to deploy RISs in communication systems, with contributions on joint beamforming [16]–[18] and robust transmission design [19], [20]. In general, the knowledge of CSI of the base station (BS)-RIS and RIS-user equipment (UE) links is needed for RIS optimization [21]. Various methods have been proposed to obtain the CSI, such as the discrete Fourier transform (DFT)-based method [22], compressed sensing (CS)-based channel estimation schemes [23]–[25], subspace-based estimation methods [26]–[28], channel estimation algorithms based on machine learning [29]. Also, several works have investigated how to deploy RISs in radar systems. Specifically, the sensing performance in

environments characterized by rich scattering can be improved through RIS beamforming [30]–[32]. For example, the authors of [33] propose a new self-sensing RIS architecture to improve the angle estimation accuracy. RISs can also be deployed in scenarios where the infrastructure, such as the Global Positioning System (GPS), is insufficient to estimate the locations of UEs and scatterers. To be specific, theoretical bounds for localization have been investigated in [34]; signal strength based localization schemes have been proposed in [35]; time-of-arrival (TOA) and angle of departure (AOD) based methods have been investigated in [36], [37].

Research on how to deploy RISs in ISAC systems is in its infancy. To enable the co-existence of radar and communication functions, the authors of [38] propose to use RISs to minimize the interference between communication and radar functions; the authors of [39] propose to deploy two RISs near the transmitter and receiver to enhance the communication signals and suppress the mutual interference. As for the design of ISAC signals, the authors of [36] show that RISs can either increase or maintain the data rate, and can offer accurate users localization and tracking performance; the authors of [40] design a low-complexity codebook which can achieve a desired localization probability of error; the authors of [41] propose to use RISs to enhance the detection performance of ISAC systems in crowded areas, while satisfying the communication signal-noise ratio (SNR) constraints; the authors of [42] point out that the degrees-of-freedom of transmit beamforming are limited when synthesizing the desired transmit beampattern and proposes to use RISs to minimize the multi-user interference. Additionally, the authors of [43] explore the performance of ISAC systems in the terahertz (THz) band. However, the scenarios considered in [38]–[43] are relatively simple.

A. The Contributions of This Work

Motivated by these available research works, we study the joint beamforming for RIS-assisted ISAC systems, considering more practical signal models that include multi-scatterer interference and multi-user interference. We first develop the signal models for the radar MI and the weighted user sum-rate. Then, we formulate two constrained optimization problems. Two algorithms are proposed to solve the formulated problems. Our proposed joint beamforming methods are shown to guarantee good performance for sensing parameter estimation and communication rate simultaneously.

The main contributions of our work are:

- We establish a more practical signal model for RIS-assisted ISAC systems, based on which the radar MI and the weighted user rate are derived.
- We formulate a joint beamforming problem for maximizing the radar MI under specified constraints for the weighted user rate, transmit power, and unit modulus reflection coefficients at the RIS. Then, an alternating optimization algorithm based on semidefinite relaxation (AO-SDR) is proposed to solve the formulated constrained optimization problem. To accelerate the convergence of AO-SDR, we introduce a method named user rate residual (URR). The algorithm is shown to provide accurate solutions for small-scale problems, i.e., the number of users is small. However, its efficiency degrades and its complexity increases quickly when the number of users becomes very large.
- To solve this issue with the AO-SDR algorithm, we propose another alternating optimization algorithm based on the Riemannian gradient (AO-RG) method. The AO-RG algorithm transforms the joint beamforming of the constrained optimization problem into a weighted optimization problem. The proposed approach can efficiently solve optimization problems for RIS-assisted ISAC beamforming systems with a large number of variables, i.e., the number of users is large.
- Simulation results are presented to verify the effectiveness of the proposed AO-SDR and AO-RG algorithms. The computational complexity of the proposed algorithms is also analyzed.

B. Paper Organization

The remainder of this paper is organized as follows. Section II introduces the system model and studies relevant performance metrics. Section III formulates the optimization models for maximizing the radar MI and introduces the AO-SDR algorithm for solving it. Section IV formulates a weighted optimization problem for maximizing the integrated radar and communication performance, and introduces the AO-RG algorithm to tackle it. Section V studies the complexity and convergence of the proposed algorithms. Section VI presents the simulation results. Section VII concludes the paper.

C. Notations

Throughout this paper, matrices are denoted by bold uppercase letters, e.g., \mathbf{S} , vectors are denoted by bold lowercase letters, e.g., \mathbf{s} , and scalars are denoted by normal fonts, e.g., s . $[\cdot]^T$

scatterer center.¹ The sets of users, RIS elements, and scatterers are denoted by \mathcal{K} , \mathcal{M} , and \mathcal{L} , respectively. The phases of the RIS elements are controlled by an RIS controller, which communicates with the DFRC BS for cooperative transmission [16].

A. Signal Model

The transmit beamforming vector and the transmit signal of the k -th user are denoted by $\mathbf{s}_k = [s_{1,k}, s_{2,k}, \dots, s_{N_t,k}]^T \in \mathbb{C}^{N_t \times 1}$ and $\mathbf{x}_k = [x_{k,1}, x_{k,2}, \dots, x_{k,N}]^T \in \mathbb{C}^{N \times 1}$, where N is the number of signal samples. The transmit beamforming matrix of the DFRC BS is $\mathbf{S} = [\mathbf{s}_1, \mathbf{s}_2, \dots, \mathbf{s}_K]$, and $\mathbf{S} \in \mathbb{C}^{N_t \times K}$. The transmit signal matrix is $\mathbf{X} = [\mathbf{x}_1, \mathbf{x}_2, \dots, \mathbf{x}_K]^T$, and $\mathbf{X} \in \mathbb{C}^{K \times N}$. The signal vectors in \mathbf{X} are assumed to be orthogonal to each other, so we have $\mathbf{X}\mathbf{X}^H = \mathbf{I}_K$. Then, the received signals at the receive antennas of the DFRC BS can be expressed as

$$\mathbf{Y}^s = \sum_{l=1}^L \left[(\mathbf{D}\Theta\mathbf{H}_l^s\Theta\mathbf{D}')^H \mathbf{S}\mathbf{X} \right] + \mathbf{W}, \quad (1)$$

where $\mathbf{Y}^s = [\mathbf{y}_1^s, \dots, \mathbf{y}_{N_r}^s]^T \in \mathbb{C}^{N_r \times N}$ is the matrix of the received signals and $\mathbf{y}_n^s \in \mathbb{C}^{N \times 1}$ is the received signal samples at the n -th antenna, $\mathbf{H}_l^s \in \mathbb{C}^{M \times M}$ is the backscattered matrix of the link between the l -th scatterer and the RIS, which is assumed to have a circularly-symmetric Gaussian random distribution according to [46], i.e., $\mathbf{H}_l^s \sim \mathcal{CN}(0, \mathbf{R}_l^s)$, and $\mathbf{H}_l^s = \alpha_l^{\text{IT}} \mathbf{G}_l^{\text{IT}}$ with $\alpha_l^{\text{IT}} = \sqrt{\frac{\lambda^2 \kappa}{64\pi^3 (d_l^{\text{IT}})^4}}$ denoting the large-scale path loss and $\mathbf{G}_l^{\text{IT}} \sim \mathcal{CN}(0, \mathbf{1}_{M \times M})$ denoting the small-scale channel matrix, where λ is the wavelength, κ is the radar cross-section (RCS) of the scatterers, and d_l^{IT} is the distance between the RIS and the l -th scatterer. Given that the RIS elements are widely separated at $\lambda/2$, the correlation between the columns of \mathbf{H}_l^s is close to zero and can be ignored, i.e., \mathbf{R}_l^s is a diagonal matrix. Moreover, $\mathbf{D} \in \mathbb{C}^{N_t \times M}$ is the channel matrix between the transmit antennas of the DFRC BS and the RIS, and it can be written as

$$\mathbf{D} = [\mathbf{d}_1^H, \mathbf{d}_2^H, \dots, \mathbf{d}_k^H, \dots, \mathbf{d}_{N_t}^H], \quad (2)$$

where $\mathbf{d}_k \in \mathbb{C}^{M \times 1}$ is the channel vector between the k -th transmit antenna and the RIS elements, and $\mathbf{D} = \beta^{\text{BI}} \mathbf{G}^{\text{BI}}$ with $\beta^{\text{BI}} = \sqrt{\frac{\lambda^2}{16\pi^2 (d^{\text{BI}})^2}}$ denoting the large-scale path loss and $\mathbf{G}^{\text{BI}} \sim \mathcal{CN}(0, \mathbf{1}_{N_t \times M})$ denoting the small-scale channel matrix, where d^{BI} is the distance between

¹In practice, the spatial distribution of the scatterers is unknown. However, we assume that the scatterers have been detected by beam tracking [44], and we need to observe the scatterers further to estimate relevant parameters, such as distance, velocity, and angle.

the transmit antennas array at the BS and the RIS. Moreover, $\mathbf{D}' \in \mathbb{C}^{M \times N_r}$ is the channel matrix between the receive antennas of the DFRC BS and the RIS elements, it can be written as

$$\mathbf{D}' = \left[(\mathbf{d}'_1)^H, (\mathbf{d}'_2)^H, \dots, (\mathbf{d}'_m)^H, \dots, (\mathbf{d}'_M)^H \right], \quad (3)$$

where $\mathbf{d}'_m \in \mathbb{C}^{N_r \times 1}$ is the channel vector between the m -th RIS element and the receive antennas, and $\mathbf{D}' = \beta^{\text{IB}} \mathbf{G}^{\text{IB}}$ with $\beta^{\text{IB}} = \sqrt{\frac{\lambda^2}{16\pi^2(d^{\text{IB}})^2}}$ denoting the large-scale path loss and $\mathbf{G}^{\text{IB}} \sim \mathcal{CN}(0, \mathbf{1}_{M \times N_r})$ denoting the small-scale channel matrix, where d^{IB} is the distance between the RIS and the receive antennas array of the BS.² In addition, Θ denotes the beamforming matrix of the RIS, which is given by

$$\Theta = \text{diag}(\theta_1^H, \theta_2^H, \dots, \theta_m^H, \dots, \theta_M^H), \quad (4)$$

where θ_m is the phase shift of the m -th RIS element. Moreover, \mathbf{W} is the additive white Gaussian noise (AWGN) at the receive antennas of the DFRC BS, with $\mathbf{W} \sim \mathcal{CN}(0, \mathbf{R}_W)$, and $\mathbf{R}_W \in \mathbb{C}^{N \times N}$ is also a diagonal matrix.

Remark 1: The received signals in (1) consist of two parts: the RIS-aided links that are backscattered by the scatterers and the AWGN. Note that we assume that the signals of the direct links between the BS and the scatterers/users are blocked. This is likely to occur for transmission in high frequency bands, such as in the millimeter-wave (mm-wave) frequency region. Meanwhile, it is reasonable to assume that there are line-of-sight (LOS) links between the BS and the RIS, between the RIS and the scatterers, and between the RIS and the UEs, provided that the RIS is properly deployed.

The received signals at the k -th user can be formulated as

$$\begin{aligned} \mathbf{y}_k^c &= (\mathbf{D}\Theta\mathbf{h}_k^{\text{IU}})^H \mathbf{s}_k \mathbf{x}_k^T + \sum_{i=1, i \neq k}^K (\mathbf{D}\Theta\mathbf{h}_k^{\text{IU}})^H \mathbf{s}_i \mathbf{x}_i^T \\ &+ \sum_{l=1}^L \sum_{k=1}^K \left[(\mathbf{D}\Theta\mathbf{h}_{l,k}^{\text{int}})^H \mathbf{s}_k \mathbf{x}_k^T \right] + \mathbf{u}_k, \forall k \in \mathcal{K}, \end{aligned} \quad (5)$$

where $\mathbf{h}_k^{\text{IU}} \in \mathbb{C}^{M \times 1}$ is the channel vector between the RIS and the k -th user with $\mathbf{h}_k^{\text{IU}} \sim \mathcal{CN}(0, \mathbf{r}_k^{\text{IU}})$, and $\mathbf{h}_k^{\text{IU}} = \beta_k^{\text{IU}} \mathbf{g}_k^{\text{IU}}$ with $\beta_k^{\text{IU}} = \sqrt{\frac{\lambda^2}{16\pi^2(d_k^{\text{IU}})^2}}$ denoting the large-scale path loss and

²Herein, we assume that the channels between the BS and the RIS, i.e., \mathbf{D} and \mathbf{D}' , are quasi-static since the BS and the RIS are stationary. The channels between the RIS and the scatterers/UEs, i.e., \mathbf{H}_l^s and \mathbf{h}_k^{IU} , are mobile since the scatterers and the UEs are mobile.

$\mathbf{g}_k^{\text{IU}} \sim \mathcal{CN}(0, \mathbf{1}_M)$ denoting the small-scale channel matrix, where d_k^{IU} is the distance between the RIS and the k -th UE. The RIS-reflected interfering product (cascaded) channel between the RIS, the l -th scatterer and the k -th user is denoted by $\mathbf{h}_{l,k}^{\text{int}} \in \mathbb{C}^{M \times 1}$ with $\mathbf{h}_{l,k}^{\text{int}} \sim \mathcal{CN}(0, \mathbf{r}_{l,k}^{\text{int}})$, and $\mathbf{h}_{l,k}^{\text{int}} = \alpha_{l,k}^{\text{TU}} \mathbf{g}_{l,k}^{\text{TU}}$ with $\alpha_{l,k}^{\text{TU}} = \sqrt{\frac{\lambda^2 \kappa}{64\pi^3 (d_l^{\text{TU}})^2 (d_{l,k}^{\text{TU}})^2}}$ denoting the large-scale path loss and $\mathbf{g}_{l,k}^{\text{TU}} \sim \mathcal{CN}(0, \mathbf{1}_M)$ denoting the small-scale channel gain, where $d_{l,k}^{\text{TU}}$ is the distance between the l -th scatterer and the k -th UE. The AWGN is denoted by \mathbf{u}_k with $\mathbf{u}_k \sim \mathcal{CN}(0, \mathbf{r}_{u_k})$.

Reamrk 2: All the channels are assumed to be perfectly estimated. The received signals of the k -th user consist of four parts: the useful signals, the interfering signals from other users, the interfering signals received from the scatterers, and the AWGN.

B. Radar Mutual Information

Assume that the transmitted waveform $\mathbf{S}\mathbf{X}$ is known [45]. The MI between the channel of the scatterers and the received echo can be expressed as

$$\begin{aligned} I(\mathbf{Y}^s; \mathbf{H}^s | \mathbf{S}\mathbf{X}) &\triangleq h(\mathbf{Y}^s | \mathbf{S}\mathbf{X}) - h(\mathbf{Y}^s | \mathbf{H}^s, \mathbf{S}\mathbf{X}) \\ &= h(\mathbf{Y}^s | \mathbf{S}\mathbf{X}) - h(\mathbf{W}). \end{aligned} \quad (6)$$

The differential entropy $h(\mathbf{Y}^s | \mathbf{S}\mathbf{X})$ and $h(\mathbf{W})$ are derived in Appendix A. Accordingly, the radar MI $I(\mathbf{Y}^s; \mathbf{H}^s | \mathbf{S}\mathbf{X})$ can be expressed as

$$I(\mathbf{Y}^s; \mathbf{H}^s | \mathbf{S}\mathbf{X}) = N_r \left\{ \log \left[\det \left(\sum_{l=1}^L \Lambda_l + \mathbf{R}_W \right) \right] - \log [\det(\mathbf{R}_W)] \right\}, \quad (7)$$

where

$$\Lambda_l = \mathbf{X}^H \mathbf{S}^H \mathbf{D} \mathbf{R}_l^s \Sigma \mathbf{D}^H \mathbf{S} \mathbf{X}, \forall l \in \mathcal{L}, \quad (8)$$

and

$$\Sigma = \text{diag} \left(\|\mathbf{d}'_1\|^2, \|\mathbf{d}'_2\|^2, \dots, \|\mathbf{d}'_M\|^2 \right). \quad (9)$$

Note that Λ_l in (8) is a diagonal matrix if \mathbf{S} is an orthogonal matrix.³ The radar MI (7) can

³The orthogonality between the columns of \mathbf{S} can be neglected first. We can use the method in [6] to project \mathbf{S} as an orthogonal matrix after we obtain the optimal \mathbf{S} by the techniques proposed in the next sections.

be rewritten as

$$\begin{aligned}
I(\mathbf{Y}^s; \mathbf{H}^s | \mathbf{S}\mathbf{X}) &= N_r \left\{ \log \prod_{k=1}^K \left[\sum_{l=1}^L \lambda_{k,l} + (\mathbf{R}_W)_{k,k} \right] \prod_{k=K+1}^N [(\mathbf{R}_W)_{k,k}] - \log \prod_{n=1}^N [(\mathbf{R}_W)_{n,n}] \right\} \\
&= N_r \left\{ \sum_{k=1}^K \log \left[\sum_{l=1}^L \lambda_{k,l} + (\mathbf{R}_W)_{k,k} \right] - \sum_{k=1}^K \log (\mathbf{R}_W)_{k,k} \right\}, \tag{10}
\end{aligned}$$

where

$$\lambda_{k,l} = \text{tr}(\mathbf{s}_k \mathbf{s}_k^H \mathbf{D} \mathbf{R}_l^s \Sigma \mathbf{D}^H), \forall k \in \mathcal{K}, \forall l \in \mathcal{L}. \tag{11}$$

C. Weighted User Sum-Rate

The average interference plus noise power for the k -th user can be formulated from (5) as

$$\zeta_k = \sum_{i=1, i \neq k}^K \left| (\mathbf{D} \Theta \mathbf{h}_k^{\text{IU}})^H \mathbf{s}_i \right|^2 + \sum_{l=1}^L \sum_{j=1}^K \left| (\mathbf{D} \Theta \mathbf{h}_{l,j}^{\text{int}})^H \mathbf{s}_j \right|^2 + \sigma_{u_k}^2, \tag{12}$$

where the average signal power of the i -th user $\|\mathbf{x}_i\|^2$ is equal to one and $\sigma_{u_k}^2$ is the variance of the AWGN \mathbf{u}_k . Then, the weighted communication rate for the k -th user [46] can be written as

$$R_k = \alpha_k \log \left(1 + \frac{1}{\zeta_k} \left| (\mathbf{D} \Theta \mathbf{h}_k^{\text{IU}})^H \mathbf{s}_k \right|^2 \right), \forall k \in \mathcal{K}, \tag{13}$$

where α_k is the weighting factor for the k -th user, and $\frac{1}{\alpha_1} + \dots + \frac{1}{\alpha_K} = 1$.

III. JOINT BEAMFORMING FOR CONSTRAINED RADAR MUTUAL INFORMATION MAXIMIZATION

In this section, a beamforming optimization problem is formulated to maximize the radar MI under specified constraints for the weighted user rate, total transmit power, and unit modulus reflection coefficients at the RIS. Then, an AO-SDR algorithm is proposed to solve the optimization problem.

A. Problem Formulation

The beamforming optimization problem for maximizing the radar MI is formulated as

$$\max_{\mathbf{S}, \Theta} \sum_{k=1}^K \log \left[\sum_{l=1}^L \lambda_{k,l} + (\mathbf{R}_W)_{k,k} \right] \quad (14a)$$

$$\text{s.t. } R_k \geq R_0, \forall k \in \mathcal{K}, \quad (14b)$$

$$\text{tr}(\mathbf{S}\mathbf{S}^H) \leq P_0, \quad (14c)$$

$$|\theta_m| = 1, \forall m \in \mathcal{M}. \quad (14d)$$

In the above problem, the constant terms, i.e., N_r and $\sum_{k=1}^K \log(\mathbf{R}_W)_{k,k}$, are omitted; (14b) is the weighted user rate constraint, and R_0 is the minimum required threshold for the user rate; (14c) is the total transmit power constraint, and P_0 is transmit power budget; (14d) is the unit modulus constraint for the reflection coefficients at the RIS. Note that the constraints (14b) and (14d) are non-convex. We propose an AO algorithm to solve the problem in (14a), which solves the transmit beamforming subproblem and the RIS beamforming subproblem iteratively.

B. Transmit Beamforming

In this subsection, the RIS beamforming matrix is kept fixed. Then, the transmit beamforming problem is formulated as a standard semidefinite programming (SDP) problem, which can be solved via the SDR method. Given the RIS beamforming matrix, specifically, the transmit beamforming problem can be formulated as

$$\max_{\{\mathbf{s}_k\}} \sum_{k=1}^K \log \left(\sum_{l=1}^L \lambda_{k,l} + (\mathbf{R}_W)_{k,k} \right) \quad (15a)$$

$$\text{s.t. } R_k \geq R_0, \forall k \in \mathcal{K}, \quad (15b)$$

$$\sum_{k=1}^K \text{tr}(\mathbf{s}_k \mathbf{s}_k^H) \leq P_0. \quad (15c)$$

Define $\mathbf{\Gamma}_k = \mathbf{s}_k \mathbf{s}_k^H$ and

$$\lambda'_{k,l} = \text{tr}(\mathbf{\Gamma}_k \mathbf{D} \mathbf{R}_l^s \mathbf{\Sigma} \mathbf{D}^H), \forall k \in \mathcal{K}, \forall l \in \mathcal{L}. \quad (16)$$

Then, the transmit beamforming problem can be reformulated as

$$\max_{\{\mathbf{\Gamma}_k\}} \sum_{k=1}^K \log \left(\sum_{l=1}^L \lambda'_{k,l} + \mathbf{R}_{k,k}^W \right) \quad (17a)$$

$$\text{s.t. } \bar{R}_k \geq R_0, \forall k \in \mathcal{K}, \quad (17b)$$

$$\sum_{k=1}^K \text{tr}(\mathbf{\Gamma}_k) \leq P_0, \quad (17c)$$

$$\text{rank}(\mathbf{\Gamma}_k) = 1, \forall k \in \mathcal{K}, \quad (17d)$$

where

$$\bar{R}_k = \alpha_k \log \left(1 + \frac{\xi_k}{\zeta_k} \right), \forall k \in \mathcal{K}, \quad (18)$$

$$\xi_k = \text{tr} \left[(\mathbf{D}\Theta \mathbf{h}_k^{\text{IU}})^H \mathbf{\Gamma}_k (\mathbf{D}\Theta \mathbf{h}_k^{\text{IU}}) \right], \forall k \in \mathcal{K}, \quad (19)$$

and

$$\bar{\zeta}_k = \text{tr} \left\{ \sum_{i=1, i \neq k}^K (\mathbf{D}\Theta \mathbf{h}_i^{\text{IU}})^H \mathbf{\Gamma}_i (\mathbf{D}\Theta \mathbf{h}_i^{\text{IU}}) \right\} + \text{tr} \left\{ \sum_{l=1}^L \sum_{j=1}^K (\mathbf{D}\Theta \mathbf{h}_{l,j}^{\text{int}})^H \mathbf{\Gamma}_j (\mathbf{D}\Theta \mathbf{h}_{l,j}^{\text{int}}) \right\} + \sigma_{u_k}^2. \quad (20)$$

The problem in (17a) can be transformed to a SDP problem by omitting the (17d) constraint, which can be directly solved using the CVX.

Remark 3: The SDR method just considered here is not tight, in general, since the problem in (17a) has multiple constraints. The rank-1 approximation method, such as the Gaussian randomization [16], is shown to provide a solution of rank one, which can be decomposed to obtain the transmit beamforming vectors. Nevertheless, the approximated solution induces some performance loss. Furthermore, it is noteworthy that the optimization variables are complex vectors in the problem (15a), but the variables are matrices in the problem (17a). The SDR method incurs an extra computational burden. Therefore, although the SDR method is the classic method to solve quadratically constrained quadratic programs (QCQP), it may not obtain the optimal solution, and the computational burden is high when the number of optimization variables is large.

C. RIS Beamforming

We now solve the RIS beamforming problem, assuming given and fixed the transmit beamforming. To accelerate the convergence of the proposed AO algorithm, we introduce a method named URR, which can reduce the search space of the RIS beamforming. We formulate the RIS beamforming as a standard SDP problem based on the URR, which can be solved via the SDR method. The RIS beamforming problem can be written as

$$\max_{\Theta} \sum_{k=1}^K \log \left[\sum_{l=1}^L \lambda_{k,l} + (\mathbf{R}_W)_{k,k} \right] \quad (21a)$$

$$\text{s.t. } R_k \geq R_0, \forall k \in \mathcal{K}, \quad (21b)$$

$$|\Theta_{m,m}| = 1, \forall m \in \mathcal{M}. \quad (21c)$$

It can be observed that the phase shifts of the RIS elements do not affect the objective function in (21a). The RIS beamforming is a feasibility-check problem. The URR method is applied to accelerate the convergence of the AO algorithm, as detailed below. The basic idea is that the URR can primarily reduce the search space in each iteration of the AO algorithm and simultaneously ensures the convergence of the AO algorithm. The RIS beamforming can be reformulated as

$$\max_{\boldsymbol{\theta}, \{\beta_k\}} \sum_{k=1}^K \beta_k \quad (22a)$$

$$\text{s.t. } \boldsymbol{\theta}^H \mathbf{a}_k + \mathbf{a}_k^H \boldsymbol{\theta} + \boldsymbol{\theta}^H \mathbf{a}_k \mathbf{a}_k^H \boldsymbol{\theta} \geq \chi_k \tilde{\zeta}_k, \forall k \in \mathcal{K}, \quad (22b)$$

$$|\boldsymbol{\theta}_m| = 1, \forall m \in \mathcal{M}, \quad (22c)$$

$$\beta_k \geq 0, \forall k \in \mathcal{K}, \quad (22d)$$

where

$$\mathbf{a}_k = \text{diag} \left[(\mathbf{h}_k^{\text{IU}})^H \right] \mathbf{D}^H \mathbf{s}_k, \forall k \in \mathcal{K}, \quad (23)$$

$\chi_k = 2^{(R_0 + \beta_k)/\alpha_k - 1}$, and

$$\tilde{\zeta}_k = \sum_{i=1, i \neq k}^K (\boldsymbol{\theta}^H \mathbf{b}_{ki} + \mathbf{b}_{ki}^H \boldsymbol{\theta} + \boldsymbol{\theta}^H \mathbf{b}_{ki} \mathbf{b}_{ki}^H \boldsymbol{\theta}) + \sum_{l=1}^L \sum_{j=1}^K (\boldsymbol{\theta}^H \mathbf{c}_{lj} + \mathbf{c}_{lj}^H \boldsymbol{\theta} + \boldsymbol{\theta}^H \mathbf{c}_{lj} \mathbf{c}_{lj}^H \boldsymbol{\theta}) + \sigma_{u_k}^2, \quad (24)$$

where

$$\mathbf{b}_{ki} = \text{diag} \left[(\mathbf{h}_k^{\text{IU}})^H \right] \mathbf{D}^H \mathbf{s}_i, \forall k \in \mathcal{K}, \quad (25)$$

and

$$\mathbf{c}_{lj} = \text{diag} \left[(\mathbf{h}_{l,j}^{\text{int}})^H \right] \mathbf{D}^H \mathbf{s}_j, \forall k \in \mathcal{K}. \quad (26)$$

An auxiliary variable t is introduced to transform the inhomogeneous quadratically constrained program (QCP) problem (22a) to a homogeneous QCP problem. Problem (22a) can be equivalently written as

$$\max_{\bar{\boldsymbol{\theta}}, \{\beta_k\}} \sum_{k=1}^K \beta_k \quad (27a)$$

$$\text{s.t. } \bar{\boldsymbol{\theta}}^H \mathbf{G}_k \bar{\boldsymbol{\theta}} \geq \chi_k \hat{\zeta}_k, \forall k \in \mathcal{K}, \quad (27b)$$

$$|\bar{\boldsymbol{\theta}}_m| = 1, \forall m \in \mathcal{M}, \quad (27c)$$

$$\beta_k \geq 0, \forall k \in \mathcal{K}, \quad (27d)$$

where

$$\bar{\boldsymbol{\theta}} = \begin{bmatrix} \boldsymbol{\theta} \\ t \end{bmatrix}, \mathbf{G}_k = \begin{bmatrix} \mathbf{a}_k \mathbf{a}_k^H & \mathbf{a}_k \\ \mathbf{a}_k^H & 0 \end{bmatrix}, \quad (28)$$

and

$$\hat{\zeta}_k = \sum_{i=1, i \neq k}^K (\bar{\boldsymbol{\theta}}^H \bar{\mathbf{G}}_{ki} \bar{\boldsymbol{\theta}}) + \sum_{l=1}^L \sum_{j=1}^K (\bar{\boldsymbol{\theta}}^H \tilde{\mathbf{G}}_{lj} \bar{\boldsymbol{\theta}}) + \sigma_{u_k}^2, \quad (29)$$

where

$$\bar{\mathbf{G}}_{ki} = \begin{bmatrix} \mathbf{b}_{ki} \mathbf{b}_{ki}^H & \mathbf{b}_{ki} \\ \mathbf{b}_{ki}^H & 0 \end{bmatrix}, \tilde{\mathbf{G}}_k = \begin{bmatrix} \mathbf{c}_{lj} \mathbf{c}_{lj}^H & \mathbf{c}_{lj} \\ \mathbf{c}_{lj}^H & 0 \end{bmatrix}. \quad (30)$$

Then, we transform the problem (27a) into a SDP problem using the SDR method. The problem (27a) can be equivalently reformulated as

$$\max_{\bar{\boldsymbol{\Theta}}, \{\beta_k\}} \sum_{k=1}^K \beta_k \quad (31a)$$

$$\text{s.t. } \text{tr}(\mathbf{G}_k \bar{\boldsymbol{\Theta}}) \geq \chi_k \hat{\zeta}'_k, \forall k \in \mathcal{K}, \quad (31b)$$

$$\bar{\boldsymbol{\Theta}}_{m,m} = 1, \forall m \in \mathcal{M}, \quad (31c)$$

$$\bar{\boldsymbol{\Theta}} \succeq 0, \quad (31d)$$

$$\beta_k \geq 0, \forall k \in \mathcal{K}, \quad (31e)$$

Algorithm 1 Alternating Optimization (AO) Algorithm to Maximize the Radar MI.

1. **Inputs:** $N_t, N_r, M, K, L, \mathbf{R}_i^s, \mathbf{D}, \mathbf{\Sigma}, \mathbf{R}_W, \alpha_k, \mathbf{h}_k^{\text{U}}, \mathbf{h}_{l,j}^{\text{int}}, \sigma_{u_k}^2, R_0, P_0, i_{\max}, \epsilon$.
 2. **Outputs:** Beamforming matrices \mathbf{S}^* and $\mathbf{\Theta}^*$ for (15a) and (22a), respectively.
 3. **Initialization:** Randomly initialize $\mathbf{S}^{(1)}, \boldsymbol{\theta}^{(1)}$, compute: $\delta^{(1)}$ according to (14a), set $\delta^{(0)} = 0, i = 0$.
 - while** $i \leq i_{\max}$, and $\delta^{(i)} - \delta^{(i-1)} \geq \epsilon$ **do**
 4. Fix $\boldsymbol{\theta}^{(i)}$, solve the convex problem (17a).
 - if** Constraint (17d) is satisfied **then**
 5. Obtain $\mathbf{S}^{(i+1)}$ directly.
 - else**
 6. Perform Gaussian randomization to obtain $\mathbf{S}^{(i+1)}$.
 - end if**
 7. Fix $\mathbf{S}^{(i+1)}$, solve the convex problem (31a).
 - if** rank-1 constraint is satisfied **then**
 8. Obtain $\boldsymbol{\theta}^{(i+1)}$ directly.
 - else**
 9. Perform Gaussian randomization to obtain $\boldsymbol{\theta}^{(i+1)}$.
 - end if**
 10. $i = i + 1$.
 - end while**
 11. $\mathbf{S}^* = \mathbf{S}^{(i)}, \mathbf{\Theta}^* = \mathbf{\Theta}^{(i)}$.
-

where $\bar{\boldsymbol{\Theta}} = \bar{\boldsymbol{\theta}}\bar{\boldsymbol{\theta}}^H$ and

$$\hat{\zeta}_k^t = \sum_{i=1, i \neq k}^K [\text{tr}(\bar{\mathbf{G}}_{ki} \bar{\boldsymbol{\Theta}})] + \sum_{l=1}^L \sum_{j=1}^K [\text{tr}(\tilde{\mathbf{G}}_{lj} \bar{\boldsymbol{\Theta}})] + \sigma_{u_k}^2. \quad (32)$$

Similar to the transmit beamforming, the SDR method applied here is not tight since the problem has multiple constraints. The proposed AO algorithm is presented in **Algorithm 1**, where $\delta^{(i)}$ is the objective value in each iteration, and ϵ is a small threshold. Also, \mathbf{S}^* and $\mathbf{\Theta}^*$ are the optimal DFRC BS beamforming matrix and the optimal RIS beamforming matrix, respectively.

IV. JOINT BEAMFORMING ON MANIFOLD

The SDR method proposed in Section III has a high computational complexity when the number of DFRC BS antennas or the RIS elements is large, such as 128 or 256. In addition, it may become infeasible when there are more users than the transmit antennas of the DFRC BS. To tackle these issues, we introduce a joint beamforming method on the manifold. First, a weighted optimization problem is formulated, where the transmit beamforming and the RIS beamforming are coupled. We transform the transmit beamforming and RIS beamforming to optimization problems on the complex hypersphere manifold and the complex circle manifold, respectively. Then, an AO-RG algorithm is introduced to solve the weighted optimization problem iteratively.

A. Problem Formulation

The weighted beamforming problem is expressed as

$$\max_{\mathbf{S}, \Theta} \frac{I(\mathbf{Y}^s; \mathbf{H}^s | \mathbf{S})}{I_{\max}} - \sum_{k=1}^K \frac{|R_k - R_0|^2}{R_0^2} \quad (33a)$$

$$\text{s.t.} \quad \text{tr}[\mathbf{S}\mathbf{S}^H] \leq P_0, \quad (33b)$$

$$|\theta_m| = 1, \forall m \in \mathcal{M}, \quad (33c)$$

where (33a) is to maximize the normalized MI and minimize the normalized mean-squared-error (MSE) of the user sum-rate; (33b) is the transmit power constraint; (33c) is the unit modulus reflection coefficients constraint at the RIS. Because the transmit beamforming and the RIS beamforming are coupled in (33a), an AO-RG algorithm is proposed to solve (33a).

B. Transmit Beamforming on the Complex Hypersphere Manifold

The first step of the proposed AO algorithm is to fix the RIS beamforming matrix. Then, the transmit beamforming problem can be formulated as

$$\max_{\mathbf{S} \in \mathcal{M}_1} \frac{1}{I_{\max}} \sum_{k=1}^K \log \left(\sum_{l=1}^L \lambda_{k,l} + \mathbf{R}_{k,k}^W \right) - \sum_{k=1}^K \frac{|R_k - R_0|^2}{R_0^2}, \quad (34)$$

which is an optimization problem on the complex hypersphere manifold \mathcal{M}_1 , $\mathcal{M}_1 = \{\mathbf{S} \in \mathbb{C}^{N_t \times K} : \|\mathbf{S}\|_F = \sqrt{P_0}\}$, where $\mathbf{S} = [\mathbf{s}_1, \dots, \mathbf{s}_K]$ and $\|\mathbf{S}\|_F = \sum_{k=1}^K \text{tr}(\mathbf{s}_k \mathbf{s}_k^H)$. The constant terms of the radar MI are omitted in (34). Next, we solve the problem (34) via a Riemannian steepest ascent (RSA) algorithm.

For any point $\mathbf{S} \in \mathcal{M}_1$, a *tangent vector* at \mathbf{S} is defined as the vector that is tangential to any smooth curves on \mathcal{M}_1 through \mathbf{S} . All the tangent vectors span the *tangent space*. For the complex hypersphere manifold \mathcal{M}_1 , the tangent space at \mathbf{S} is defined as

$$T_{\mathbf{S}}\mathcal{M}_1 \triangleq \{\mathbf{Z} \in \mathbb{C}^{N_t \times K} : \text{Re}\{\text{tr}(\mathbf{S}^H \mathbf{Z})\} = 0\}. \quad (35)$$

Let $g(\mathbf{S}) \triangleq g_1(\mathbf{S}) - g_2(\mathbf{S})$ be the objective function of problem (34), with

$$g_1(\mathbf{S}) = \frac{1}{I_{\max}} \sum_{k=1}^K \log \left(\sum_{l=1}^L \lambda_{k,l} + \mathbf{R}_{k,k}^W \right) \quad (36)$$

and

$$g_2(\mathbf{S}) = \frac{1}{R_0^2} \cdot \sum_{k=1}^K \left| \alpha_k \log_2 \left(1 + \frac{1}{\zeta_k} \left| (\mathbf{D}\Theta \mathbf{h}_k^{\text{IU}})^H \mathbf{s}_k \right|^2 \right) - R_0 \right|^2. \quad (37)$$

The Euclidean gradient of $g(\mathbf{S})$ is

$$\nabla_{\mathbf{s}} g = \left[\frac{\partial g_1}{\partial \mathbf{s}_1} - \frac{\partial g_2}{\partial \mathbf{s}_1}, \dots, \frac{\partial g_1}{\partial \mathbf{s}_k} - \frac{\partial g_2}{\partial \mathbf{s}_k}, \dots, \frac{\partial g_1}{\partial \mathbf{s}_K} - \frac{\partial g_2}{\partial \mathbf{s}_K} \right], \quad (38)$$

where

$$\frac{\partial g_1}{\partial \mathbf{s}_k} = \frac{2}{I_{\max} \ln 2} \cdot \sum_{l=1}^L \left[\frac{(\mathbf{D}\mathbf{R}_l^S \Sigma \mathbf{D}^H) \mathbf{s}_k}{\lambda_{k,l} + \mathbf{R}_{k,k}^W} \right] \quad (39)$$

and

$$\frac{\partial g_2}{\partial \mathbf{s}_k} = \frac{2}{R_0^2 \ln 2} \left[\alpha_k \log_2 \left(1 + \frac{\psi_k}{\zeta_k} \right) - R_0 \right] \cdot \left[\frac{\alpha_k}{(\zeta_k + \psi_k)} \cdot \frac{\partial \psi_k}{\partial \mathbf{s}_k} - \sum_{n=1}^K \frac{\alpha_n}{(\zeta_n + \psi_n)} \cdot \frac{\psi_n}{\zeta_n} \cdot \frac{\partial \zeta_n}{\partial \mathbf{s}_k} \right], \quad (40)$$

where

$$\psi_k = \left| (\mathbf{D}\Theta \mathbf{h}_k^{\text{IU}})^H \mathbf{s}_k \right|^2, \quad (41)$$

$$\frac{\partial \psi_k}{\partial \mathbf{s}_k} = 2 \mathbf{D}\Theta \mathbf{h}_k^{\text{IU}} (\mathbf{D}\Theta \mathbf{h}_k^{\text{IU}})^H \mathbf{s}_k, \quad (42)$$

and

$$\frac{\partial \zeta_n}{\partial \mathbf{s}_k} = \begin{cases} 2 \sum_{l=1}^L \left[\mathbf{D}\Theta \mathbf{h}_{l,k}^{\text{int}} (\mathbf{D}\Theta \mathbf{h}_{l,k}^{\text{int}})^H \mathbf{s}_k \right], & n = k, \\ \frac{\partial \psi_k}{\partial \mathbf{s}_k} + 2 \sum_{l=1}^L \left[\mathbf{D}\Theta \mathbf{h}_{l,k}^{\text{int}} (\mathbf{D}\Theta \mathbf{h}_{l,k}^{\text{int}})^H \mathbf{s}_k \right], & n \neq k. \end{cases} \quad (43)$$

In order to derive the Riemannian gradient, we need to project the Euclidean gradient of the problem (34) onto the *tangent space* (35). The projection procedure is defined as

$$\text{grad}_{\mathcal{S}} g \triangleq \nabla_{\mathcal{S}} g - \text{Re} \{ \text{tr} (\mathbf{S}^H \nabla_{\mathbf{s}} g) \} \mathbf{S}. \quad (44)$$

Next, in order to obtain the transmit beamforming matrix on \mathcal{M}_1 , we define the iterative direction for the RSA, i.e., the iterative direction on \mathcal{M}_1 . Assume that the direction of the i -th iteration for the RSA is $\boldsymbol{\eta}_i$. Since the i -th iterative direction $\boldsymbol{\eta}_i$ and the $(i-1)$ -th iterative direction $\boldsymbol{\eta}_{i-1}$ are located in different *tangent space*, i.e., $T_{\mathcal{S}^{(i)}}$ and $T_{\mathcal{S}^{(i-1)}}$, they can not be directly added. A projection operation is needed to perform the nonlinear combination. The i -th direction is

Algorithm 2 Riemannian Steepest Ascent (RSA) Algorithm for Solving the Transmit Beamforming Subproblem.

1. **Inputs:** $N_t, N_r, M, K, L, \Theta, \mathbf{R}_l^s, \mathbf{D}, \Sigma, \mathbf{R}_W, \alpha_k, \mathbf{h}_k^{\text{IU}}, \mathbf{h}_{l,j}^{\text{int}}, \sigma_{u_k}^2, R_0, P_0, i_{\max}, \epsilon$.
 2. **Outputs:** Beamforming matrices \mathbf{S}^* for (34).
 3. **Initialization:** Randomly initialize $\mathbf{S}^{(0)} = \mathbf{S}^{(1)} \in \mathcal{M}_1$, compute $\text{grad}_{\mathbf{S}^{(0)}} g$ and $\text{grad}_{\mathbf{S}^{(1)}} g$ according to (44), set $\boldsymbol{\eta}_0 = \text{grad}_{\mathbf{S}^{(0)}} g$ and $i = 1$.
 - while** $i \leq i_{\max}$, and $\|\text{grad}_{\mathbf{S}^{(i)}} g\|_F \geq \epsilon$ **do**
 4. Calculate the difference \mathbf{J}_i according to (48).
 5. Calculate the combination factor δ_i according to (47).
 6. Calculate the search direction $\boldsymbol{\eta}_i$ according to (45).
 7. Compute $\mathbf{S}^{(i+1)}$ by the retraction projection operation (49), i.e., $\mathbf{S}^{(i+1)} = \mathcal{R}_{\mathbf{S}^{(i)}}(\mu_i \boldsymbol{\eta}_i)$, where μ_i is the step size that is computed by line search method, such as Armijo rule.
 8. $i = i + 1$.
 - end while**
 9. $\mathbf{S}^* = \mathbf{S}^{(i)}$.
-

defined as

$$\boldsymbol{\eta}_i \triangleq \text{grad}_{\mathbf{S}^{(i)}} g + \delta_i T_{\mathbf{S}^{(i-1)} \rightarrow \mathbf{S}^{(i)}}(\boldsymbol{\eta}_{i-1}), \quad (45)$$

where $T_{\mathbf{S}^{(i-1)} \rightarrow \mathbf{S}^{(i)}}(\boldsymbol{\eta}_{i-1})$ is the projection operation that projects the $(i-1)$ -th iterative direction $\boldsymbol{\eta}_{i-1}$ onto the *tangent space* of the i -th iteration $\boldsymbol{\eta}_i$, which is given as

$$\begin{aligned} T_{\mathbf{S}^{(i-1)} \rightarrow \mathbf{S}^{(i)}}(\boldsymbol{\eta}_{i-1}) &\triangleq T_{\mathbf{S}^{(i-1)}} \mathcal{M}_1 \rightarrow T_{\mathbf{S}^{(i)}} \mathcal{M}_1 \\ &\triangleq \boldsymbol{\eta}_{i-1} - \text{Re} \left\{ \text{tr} \left(\left(\mathbf{S}^{(i)} \right)^H \boldsymbol{\eta}_{i-1} \right) \right\} \mathbf{S}^{(i)}, \end{aligned} \quad (46)$$

and δ_i is the combination factor that is computed by the Polak-Ribière formula [47]. The Polak-Ribière formula is defined by

$$\delta_i \triangleq \frac{\langle \text{grad}_{\mathbf{S}^{(i)}} g, \mathbf{J}_i \rangle}{\langle \text{grad}_{\mathbf{S}^{(i-1)}} g, \text{grad}_{\mathbf{S}^{(i-1)}} g \rangle}, \quad (47)$$

where \mathbf{J}_i is the difference between the gradient of this iteration and the iterative direction of the last iteration, and \mathbf{J}_i is defined as

$$\mathbf{J}_i \triangleq \text{grad}_{\mathbf{S}^{(i)}} g - T_{\mathbf{S}^{(i-1)} \rightarrow \mathbf{S}^{(i)}}(\boldsymbol{\eta}_{i-1}). \quad (48)$$

Finally, the retraction projection is needed to project the points in the *tangent space* onto the complex hypersphere manifold during each iteration of the RSA algorithm. The retraction projection operation is defined as

$$\mathcal{R}_{\mathbf{S}}(\mathbf{Z}) \triangleq \frac{\sqrt{P_0} \cdot (\mathbf{S} + \mathbf{Z})}{|\mathbf{S} + \mathbf{Z}|_F}. \quad (49)$$

The RSA algorithm for solving the problem (34) is summarized in **Algorithm 2**.

C. RIS Beamforming on the Complex Circle Manifold

Assuming the transmit beamforming matrix fixed, the problem (33a) can be reformulated as

$$\min_{\boldsymbol{\theta} \in \mathcal{M}_2} \sum_{k=1}^K |R_k - R_0|^2, \quad (50)$$

which is an optimization problem on the complex circle manifold \mathcal{M}_2 , $\mathcal{M}_2 = \{\boldsymbol{\theta} \in \mathbb{C}^{M \times 1} : |\theta_1| = |\theta_2| = \dots = |\theta_M| = 1\}$.

Similar to the transmit beamforming, we define some essential concepts for the complex circle manifold that will be useful for solving the RIS beamforming by using a Riemannian steepest descent (RSD) algorithm. The *tangent space* of any point $\boldsymbol{\theta} \in \mathcal{M}_2$ is given as

$$T_{\boldsymbol{\theta}}\mathcal{M}_2 \triangleq \{\mathbf{z} \in \mathbb{C}^M : \text{Re}\{\mathbf{z} \circ \boldsymbol{\theta}^H\} = \mathbf{0}_M\}. \quad (51)$$

The objective function of problem (50) is

$$f(\boldsymbol{\theta}) = \sum_{k=1}^K \left| \alpha_k \log_2 \left(1 + \frac{1}{\zeta_k} |\boldsymbol{\theta}^H \mathbf{a}_k|^2 \right) - R_0 \right|^2. \quad (52)$$

Then, the Euclidean gradient of $f(\boldsymbol{\theta})$ is given by

$$\begin{aligned} \nabla_{\boldsymbol{\theta}} f &= \sum_{k=1}^K 2 \left[\alpha_k \log_2 \left(1 + \frac{1}{\zeta_k} |\boldsymbol{\theta}^H \mathbf{a}_k|^2 \right) - R_0 \right] \cdot \frac{\alpha_k}{\ln 2 \left(1 + \frac{1}{\zeta_k} |\boldsymbol{\theta}^H \mathbf{a}_k|^2 \right)} \\ &\cdot \left\{ \frac{2 (\mathbf{a}_k \mathbf{a}_k^H \boldsymbol{\theta} + \mathbf{a}_k)}{\zeta_k} - \frac{(\boldsymbol{\theta}^H \mathbf{a}_k + \mathbf{a}_k^H \boldsymbol{\theta} + \boldsymbol{\theta}^H \mathbf{a}_k \mathbf{a}_k^H \boldsymbol{\theta})}{|\zeta_k|^2} \right. \\ &\cdot \left. \left[\sum_{i=1, i \neq k}^K 2 (\mathbf{b}_{ki} \mathbf{b}_{ki}^H \boldsymbol{\theta} + \mathbf{b}_{ki}) + \sum_{l=1}^L \sum_{j=1}^K 2 (\mathbf{c}_{lj} \mathbf{c}_{lj}^H \boldsymbol{\theta} + \mathbf{c}_{ij}) \right] \right\}. \end{aligned} \quad (53)$$

We need to project the Euclidean gradient of (52) onto the *tangent space* (51) to obtain the Riemannian gradient. The projection procedure for the complex circle manifold is defined as

$$\text{grad}_{\boldsymbol{\theta}} f \triangleq \nabla_{\boldsymbol{\theta}} f - \text{Re}\{\nabla_{\boldsymbol{\theta}} f \circ \boldsymbol{\theta}^H\} \circ \boldsymbol{\theta}. \quad (54)$$

Furthermore, the i -th iterative direction of the RSD algorithm is defined as

$$\boldsymbol{\eta}_i = -\text{grad}_{\boldsymbol{\theta}^{(i)}} f + \delta_i T_{\boldsymbol{\theta}^{(i-1)} \rightarrow \boldsymbol{\theta}^{(i)}} (\boldsymbol{\eta}_{i-1}), \quad (55)$$

where $T_{\boldsymbol{\theta}^{(i-1)} \rightarrow \boldsymbol{\theta}^{(i)}} (\boldsymbol{\eta}_{i-1})$ and δ_i are the projection operation and the combination factor, respec-

Algorithm 3 Riemannian Steepest Descent (RSD) Algorithm for Solving the RIS Beamforming Subproblem.

1. **Inputs:** $N_t, N_r, M, K, L, \mathbf{S}, \mathbf{R}_i^s, \mathbf{D}, \Sigma, \mathbf{R}_W, \alpha_k, \mathbf{h}_k^{\text{IU}}, \mathbf{h}_{l,j}^{\text{int}}, \sigma_{u_k}^2, R_0, P_0, i_{\max}, \epsilon$.
 2. **Outputs:** Beamforming matrices $\boldsymbol{\theta}^*$ for (50).
 3. **Initialization:** Randomly initialize $\boldsymbol{\theta}^{(0)} = \boldsymbol{\theta}^{(1)} \in \mathcal{M}_2$, compute $\text{grad}_{\boldsymbol{\theta}^{(0)}} f$ and $\text{grad}_{\boldsymbol{\theta}^{(1)}} f$ according to (54), set $\boldsymbol{\eta}_0 = \text{grad}_{\boldsymbol{\theta}^{(0)}} f$ and $i = 1$.
 - while** $i \leq i_{\max}$, and $\|\text{grad}_{\boldsymbol{\theta}^{(i)}} f\|_F \geq \epsilon$ **do**
 4. Calculate the difference \mathbf{J}_i .
 5. Calculate the combination factor δ_i according to (57).
 6. Calculate the search direction $\boldsymbol{\eta}_i$ according to (55).
 7. Compute $\boldsymbol{\theta}^{(i+1)}$ by the retraction projection operation (58), i.e., $\boldsymbol{\theta}^{(i+1)} = \mathcal{R}_{\boldsymbol{\theta}^{(i)}}(\mu_i \boldsymbol{\eta}_i)$, where μ_i is the step size that is compute by line search method, such as Armijo rule.
 8. $i = i + 1$.
 - end while**
 9. $\boldsymbol{\theta}^* = \boldsymbol{\theta}^{(i)}$.
-

Algorithm 4 Alternating Optimization (AO) Algorithm for Solving the Weighted Optimization Problem (33a).

1. **Inputs:** $N_t, N_r, M, K, L, \mathbf{R}_i^s, \mathbf{D}, \Sigma, \mathbf{R}_W, \alpha_k, \mathbf{h}_k^{\text{IU}}, \mathbf{h}_{l,j}^{\text{int}}, \sigma_{u_k}^2, R_0, P_0, p_{\max}, \epsilon$.
 2. **Outputs:** Beamforming matrices \mathbf{S}^* and $\boldsymbol{\theta}^*$ for (34) and (50), respectively.
 3. **Initialization:** Conduct the initialization of Algorithm 2 and Algorithm 3. Compute the objective value $\zeta^{(1)}$ according to (33a), set $\zeta^{(0)} = 0, p = 0$.
 - while** $p \leq p_{\max}$, and $\zeta^{(p)} - \zeta^{(p-1)} \geq \epsilon$ **do**
 4. Fix $\boldsymbol{\theta}^{(p)}$, and solve the complex hypersphere manifold optimization problem (34) to obtain $\mathbf{S}^{(p+1)}$.
 5. Fix $\mathbf{S}^{(p+1)}$, and solve the complex circle manifold optimization problem (50) to obtain $\boldsymbol{\theta}^{(p+1)}$.
 6. $p = p + 1$.
 - end while**
 11. $\mathbf{S}^* = \mathbf{S}^{(p)}, \boldsymbol{\theta}^* = \boldsymbol{\theta}^{(p)}$.
-

tively, and they can be expressed as

$$\begin{aligned}
 T_{\boldsymbol{\theta}^{(i-1)} \rightarrow \boldsymbol{\theta}^{(i)}}(\boldsymbol{\eta}_{i-1}) &\triangleq T_{\boldsymbol{\theta}^{(i-1)}} \mathcal{M}_2 \rightarrow T_{\boldsymbol{\theta}^{(i)}} \mathcal{M}_2 \\
 &\triangleq \boldsymbol{\eta}_{i-1} - \text{Re} \left\{ \boldsymbol{\eta}_{i-1} \circ \left(\boldsymbol{\theta}^{(i)} \right)^H \right\} \circ \boldsymbol{\theta}^{(i)}
 \end{aligned} \tag{56}$$

and

$$\delta_i \triangleq \frac{\langle \text{grad}_{\boldsymbol{\theta}^{(i)}} f, \mathbf{J}_i \rangle}{\langle \text{grad}_{\boldsymbol{\theta}^{(i-1)}} f, \text{grad}_{\boldsymbol{\theta}^{(i-1)}} f \rangle}, \tag{57}$$

where \mathbf{J}_i is the difference of directions, which is similar to that in (48). Moreover, the retraction projection of the complex circle manifold is defined as

$$\mathcal{R}_{\boldsymbol{\theta}}(\mathbf{z}) \triangleq \left(\frac{z_1}{|z_1|}, \dots, \frac{z_M}{|z_M|} \right)^T. \tag{58}$$

The RSD algorithm for solving the RIS beamforming problem is summarized in **Algorithm 3**, and the proposed complete AO algorithm for solving the weighted optimization problem (33a) is presented in **Algorithm 4**.

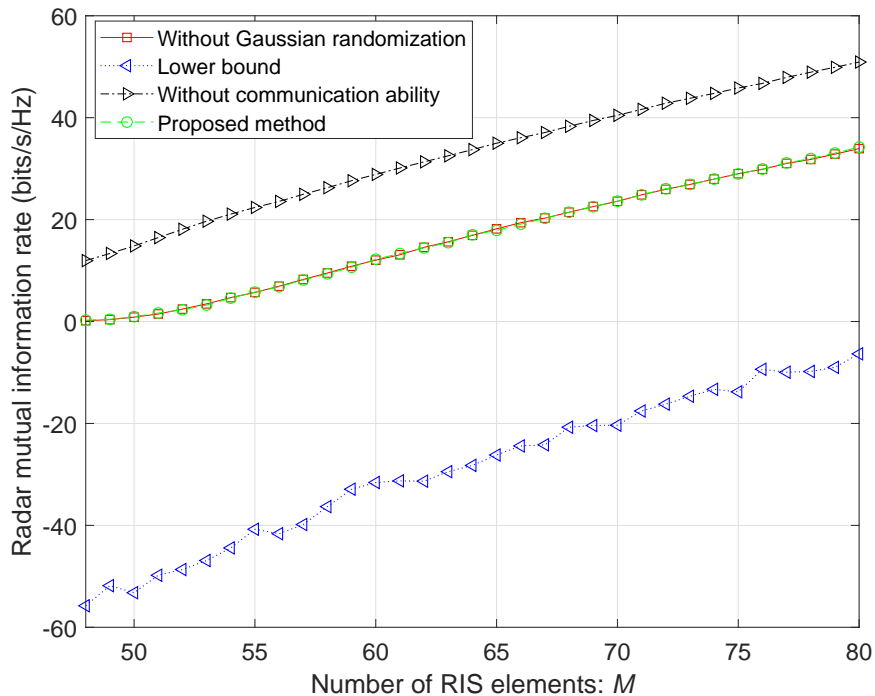


Fig. 2. Radar MI versus the number of RIS elements when the transmit power budget equals 40dBm, and the threshold of user rate R_0 equals 4 bits/s/Hz.

V. COMPLEXITY AND CONVERGENCE ANALYSIS

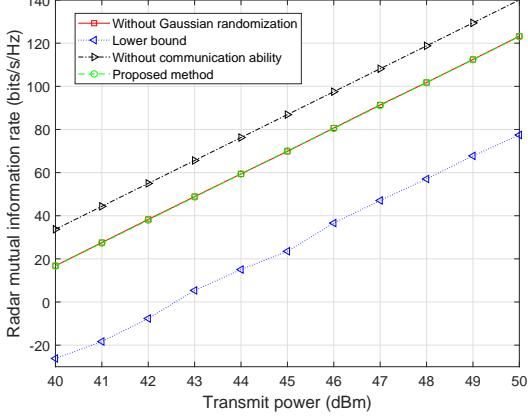
We mainly analyze the computational complexity of the SDR methods and the manifold optimization algorithms in each AO iteration since the number of the required total iterations is hard to predict. The overall complexity of the proposed methods will be verified via simulation results in the next section. We use the flops number to denote the computational complexity. A flop is defined as one real addition or one real multiplication [48].

A. Complexity Analysis for SDR Methods

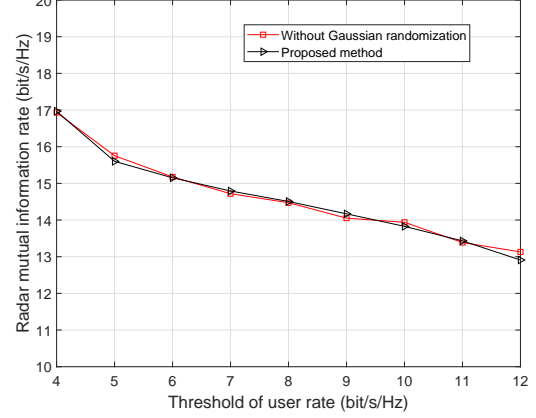
The SDR problems (17a) and (31a) can be solved with a worst-case complexity of $\mathcal{O}_{\text{SDR}}^{\text{Transmit}} = N_t^4 K^{0.5} + K^{4.5}$ and $\mathcal{O}_{\text{SDR}}^{\text{RIS}} = M^4 K^{0.5} + K^{4.5}$ [49], respectively.

B. Complexity Analysis for the RSA Algorithm

The number of iterations for the RSA algorithm (**Algorithm 2**) is generally in the range of 5 to 10. Next, we analyze the complexity for each iteration. As shown in line 4 in the RSA algorithm, the computations in each iteration are mainly for the Euclidean gradient (38),

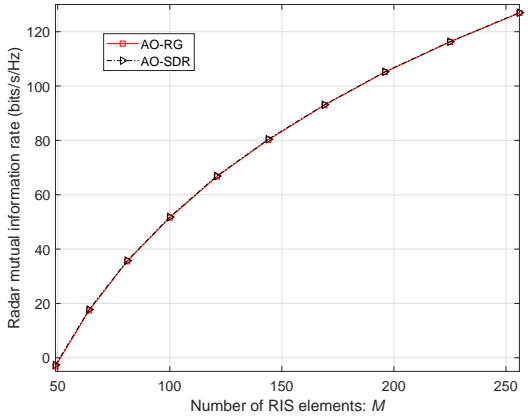


(a) Radar MI versus the transmit power budget.

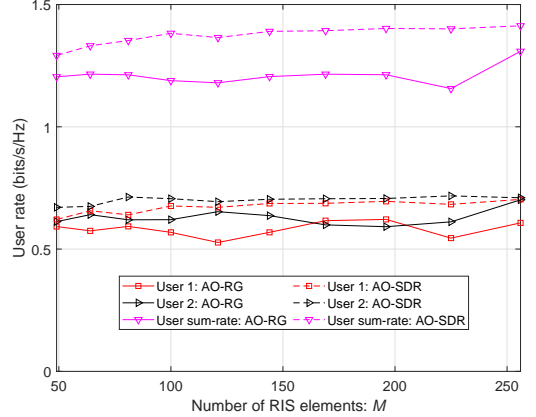


(b) Radar MI versus the weighted user rate.

Fig. 3. Radar MI versus the transmit power budget when the number of RIS elements equals 64, and the threshold of user rate R_0 equals 4 bits/s/Hz. Radar MI versus the weighted user rate when the number of RIS elements equals 64.



(a) Radar MI versus the number of RIS elements.



(b) User rate versus the number of RIS elements.

Fig. 4. Radar MI versus the number of RIS elements, when the threshold of user rate is 1 bits/s/Hz. User rate versus the number of RIS elements, when the threshold of user rate is 1 bits/s/Hz.

the Riemannian gradient (44), and the projection operation (46). Their orders of flops can be computed as $\mathcal{O}_{\text{RSA}}^{\text{EG}} = K^2 N_t (16N_t + 14M + 2) + K (16N_t^2 + 14N_t M + 8N_t + 14N_t) + (KL + K) (14N_t M + 10N_t) + KL (16N_t^2 M + 16N_t^3 + 24N_t^2 + 4N_t M + 6N_t + M)$, $\mathcal{O}_{\text{RSA}}^{\text{RG}} = 12N_t K$, and $\mathcal{O}_{\text{RSA}}^{\text{PR}} = 12N_t K$, respectively. Hence, the number of flops for calculating line 4 is $\mathcal{O}_{\text{RSA}}^{\text{Line4}} = \mathcal{O}_{\text{RSA}}^{\text{EG}} + \mathcal{O}_{\text{RSA}}^{\text{RG}} + \mathcal{O}_{\text{RSA}}^{\text{PR}} = K^2 N_t (16N_t + 14M + 2) + K (16N_t^2 + 14N_t M + 8N_t + 14N_t) + (KL + K) (14N_t M + 10N_t) + 20N_t K + KL (16N_t^2 M + 16N_t^3 + 22N_t^2 + 4N_t M + 6N_t + M)$. The complexity for calculating line 5, 6, 7 are $16N_t K$, $4N_t K$, and $12N_t K$ flops, respectively. Therefore, the total complexity of the RSA algorithm \mathcal{O}_{RSA} is $\mathcal{O}(N_t^2 K L M + N_t^3 K L)$.

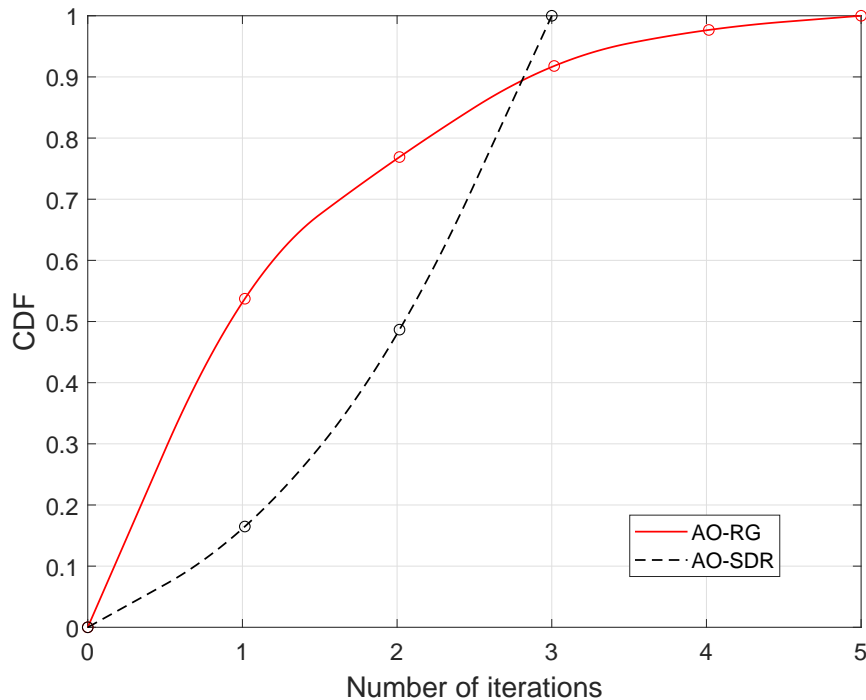


Fig. 5. The convergence performance of AO-RG algorithm, when the number of RIS elements equals 64.

C. Complexity Analysis for the RSD Algorithm

Similarly, the iterations for the RSD algorithm (**Algorithm 3**) is in the range of 2 to 10. The complexity for each iteration is analysed next. The number of flops for the Euclidean gradient (53), the Riemannian gradient (54), and the projection operation (56) are given by $\mathcal{O}_{\text{RSD}}^{\text{EG}} = K(30N_tM + 16M^2 + 26M + 16N_t) + (K + KL)(14N_tM + 16M^2 + 8N_t) + 2KM$, $\mathcal{O}_{\text{RSD}}^{\text{RG}} = 12M$, and $\mathcal{O}_{\text{RSD}}^{\text{PR}} = 12M$, respectively. Hence, the number of flops for line 4 in **Algorithm 3** is $\mathcal{O}_{\text{RSD}}^{\text{Line4}} = \mathcal{O}_{\text{RSD}}^{\text{EG}} + \mathcal{O}_{\text{RSD}}^{\text{RG}} + \mathcal{O}_{\text{RSD}}^{\text{PR}} = K(30N_tM + 16M^2 + 26M + 16N_t) + (K + KL)(14N_tM + 16M^2 + 8N_t) + 2KM + 24M$. The complexity for lines 5, 6, 7 are $16M$, $4M$, and $6M$ flops, respectively. Therefore, the complexity of the RSD algorithm \mathcal{O}_{RSD} is $\mathcal{O}(N_tKLM + M^2KL)$.

D. Convergence Analysis

In order to guarantee the convergence of AO, the sub-problem for updating each variable needs to be solved optimally in each iteration [50]. The SDR method is proposed to solve the transmit beamforming and the RIS beamforming for maximizing the radar MI. Since the

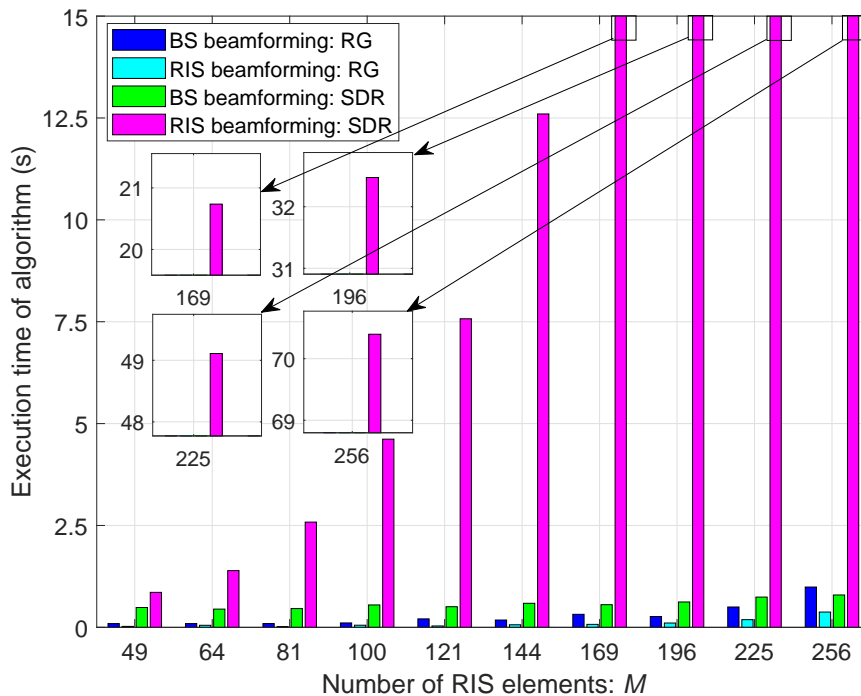


Fig. 6. The convergence time of the beamforming subproblem in each iteration of the proposed AO algorithm.

Gaussian randomization induces an extra error, the SDR method may not always be optimal. However, as will be seen from the simulation results in Section VI, the beamforming matrices obtained by the SDR satisfy the rank-1 constraint in most cases, i.e., the proposed AO-SDR algorithm is convergent. In addition, we will also show the convergence performance for the proposed AO-RG algorithm by simulation results in the next section.

VI. SIMULATION RESULTS

This section provides numerous simulation results to verify the proposed algorithms' effectiveness. We assume that the BS is located at (0m, 0m); the RIS is located at (50m, 10m); the K UEs and L scatterers are uniformly distributed in a circle with a radius of five meters centered at (70m, 0m) and (70m, 10m), respectively.

A. Results for the Proposed AO-SDR Algorithm

In order to verify the effectiveness of the proposed AO-SDR algorithm, one lower bound and two upper bounds are utilized to be compared with the proposed AO-SDR. The lower bound is the

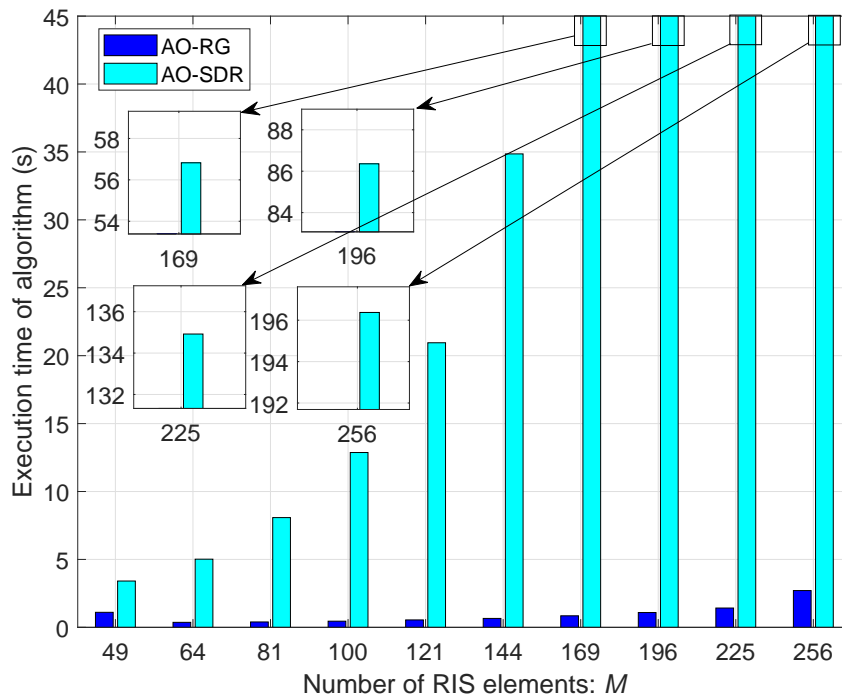


Fig. 7. The convergence performance of the proposed AO algorithm versus the number of RIS elements.

radar MI obtained by configuring the beamforming matrix randomly. The two upper bounds are the radar MI obtained by the AO-SDR algorithm without applying Gaussian randomization and the AO-SDR algorithm without the user rate constraint, i.e., without considering communication performance. From Fig. 2 to Fig. 3, the number of DFRC BS transmit antennas and receive antennas are 16, the number of scatterers is 2, the number of users is 2, the weighting factors for the user rate are both 2, and the noise power is -110dBm.

Figure 2 shows how the radar MI increases when increasing the RIS elements. The increasing trend is because the RIS provides extra signal paths, which enhance the radar echo strength. The radar MI obtained by the proposed AO-SDR method with Gaussian randomization and without Gaussian randomization are almost the same. Hence, the proposed AO-SDR algorithm can achieve the optimal solution and is convergent as discussed in Section V.C. Moreover, the radar MI obtained by the proposed AO-SDR method is smaller than that obtained by the SDR method without the user rate constraint. The reason is that the radar MI depends on the BS beamforming, which is only used to maximize the radar MI when we remove the user rate constraint.

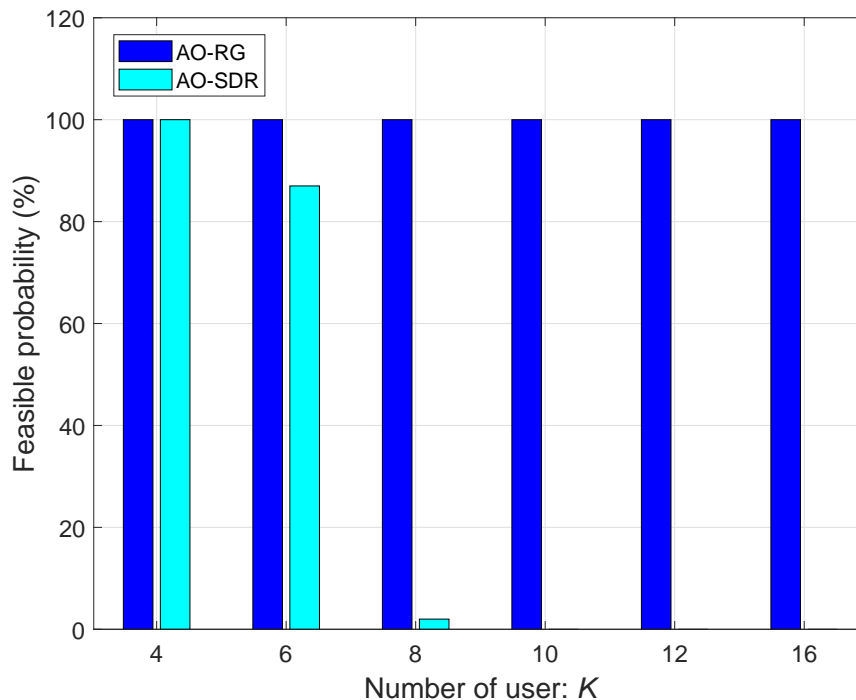


Fig. 8. The feasible probability of AO-SDR and AO-RG when the number of RIS elements is 64

Figure 3(a) demonstrates that the radar MI steadily increases as the transmit power budget increases, as the feasible region of joint beamforming becomes larger when the transmit power budget increases. Similar to Fig.2, the radar MI obtained by the proposed AO-SDR method and the AO-SDR without Gaussian randomization are almost the same, and the radar MI obtained by the proposed AO-SDR method is smaller than that obtained by the SDR method without the user rate constraint.

In Fig. 3(b), we show that the radar MI obtained by the AO-SDR algorithm decreases as the threshold of the weighted user rate increases. The reason is that the radar MI and user rate are both impacted by the BS beamforming. The degrees-of-freedom for maximizing the radar MI are limited when the threshold of weighted user rate becomes large.

B. Results for the Proposed AO-RG Algorithm

For results in this subsection, the numbers of DFRC BS transmit antennas and receive antennas are both 16. The transmit power budget is 40dBm. The number of scatterers is 2.

Figure 4(a) shows that the radar MI of the AO-RG and AO-SDR algorithms both increase as the number of RIS elements increases, and the radar MI obtained by the two methods are close. Figure 4(b) shows that the user rate obtained by the AO-RG algorithm is close to that obtained by the AO-SDR algorithm. This indicates that the weighted beamforming problem solved by the AO-RG algorithm can simultaneously satisfy the communication and sensing performances.

Figure 5 is the cumulative distribution function (CDF) of the number of iterations, and it shows that both AO-RG and AO-SDR algorithms converge within five iterations in all channel realizations. This indicates that the proposed AO-SDR algorithm converges rapidly.

In Fig. 6 and Fig. 7, the number of users K is 2, the weighting factors for user rate are both 2, and the threshold of the weighted user rate R_0 is 1. Since closed-form expressions for the computational complexity of the AO methods are difficult to obtain, the execution time is chosen to represent the time needed for solving the beamforming for one channel realization in Fig. 6 and Fig. 7. The simulations are performed on an Intel Core Xeon W-2125 4.00GHz CPU 32GB RAM computer.

In Fig. 6, we show that the convergence time of both proposed algorithms increases as the number of RIS elements increases. The RG-based algorithms for solving the BS beamforming and RIS beamforming require much less time than the SDR-based algorithms in all cases. The convergence time of the SDR-based algorithms is long when the number of RIS elements is large, e.g., 225 and 256. Conversely, the convergence time of the RG-based algorithms is stable and short, which illustrates the superiority of the RG-based algorithms. In Fig. 7, we observe that the AO-RG algorithm requires much less time than the AO-SDR algorithm in all cases, and the AO-RG algorithm shows better convergence performance than the AO-SDR algorithm when the number of RIS elements is large.

As shown in Fig. 8, the AO-RG algorithm is always feasible for any number of users since the weighted beamforming problem is an unconstrained optimization problem on the manifolds. However, the AO-SDR algorithm may be infeasible when the number of users is large because the degrees-of-freedom in the optimization are limited, and the constraints on the communication rate are difficult to satisfy.

VII. CONCLUSION

We have presented two joint beamforming techniques, AO-SDR and AO-RG, for RIS-assisted ISAC systems. The radar MI and the weighted communication user rate are jointly optimized.

The AO-SDR algorithm was proposed to maximize the radar MI under user rate constraints. In order to reduce the computational complexity and improve the feasibility, the AO-RG algorithm was proposed to solve the weighted joint beamforming problem. Simulation results demonstrate that RIS can simultaneously enhance the radar MI and the communication rate. The AO-RG algorithm was shown to outperform the AO-SDR algorithm in terms of both the execution time and the feasibility probability. Therefore, the AO-RG algorithm is superior for applications requiring high reliability and low computational latency, such as emergency rescue and military systems.

APPENDIX A

DERIVATION OF THE DIFFERENTIAL ENTROPY

The differential entropy $h(\mathbf{Y}^s|\mathbf{S}\mathbf{X})$ can be formulated as

$$h(\mathbf{Y}^s|\mathbf{S}\mathbf{X}) = \int -p(\mathbf{Y}^s|\mathbf{S}\mathbf{X}) \log [p(\mathbf{Y}^s|\mathbf{S}\mathbf{X})] d\mathbf{Y}^s, \quad (59)$$

where

$$\begin{aligned} p(\mathbf{Y}^s|\mathbf{S}\mathbf{X}) &= \prod_{n=1}^{N_r} p(\mathbf{y}_n^s|\mathbf{S}\mathbf{X}) \\ &= \prod_{n=1}^{N_r} \frac{1}{\pi^{N_r} \det \left[\sum_{l=1}^L \mathbf{\Lambda}_l + \mathbf{R}_W \right]} \times \exp \left[-\mathbf{y}_n^s \left(\sum_{l=1}^L \mathbf{\Lambda}_l + \mathbf{R}_W \right) (\mathbf{y}_n^s)^T \right] \\ &= \frac{1}{\pi^{N_r N} \det^{N_r} \left[\sum_{l=1}^L \mathbf{\Lambda}_l + \mathbf{R}_W \right]} \times \exp \left\{ -\text{tr} \left[\left(\sum_{l=1}^L \mathbf{\Lambda}_l + \mathbf{R}_W \right)^{-1} \mathbf{Y}^s (\mathbf{Y}^s)^H \right] \right\}. \end{aligned} \quad (60)$$

Thus, we have

$$h(\mathbf{Y}^s|\mathbf{S}\mathbf{X}) = N_r N \log(\pi) + N_r N + N_r \log \left[\det \left(\sum_{l=1}^L \mathbf{\Lambda}_l + \mathbf{R}_W \right) \right]. \quad (61)$$

The differential entropy $h(\mathbf{W})$ can be written as

$$h(\mathbf{W}) = \int -p(\mathbf{W}) \log [p(\mathbf{W})] d\mathbf{W}, \quad (62)$$

where

$$p(\mathbf{W}) = \frac{1}{\pi^{N_r N} \det^{N_r}(\mathbf{W})} \exp \left\{ -\text{tr} \left[(\mathbf{R}_W)^{-1} \mathbf{W} \mathbf{W}^H \right] \right\}. \quad (63)$$

Then, the differential entropy $h(\mathbf{W})$ is

$$h(\mathbf{W}) = N_r N \log(\pi) + N_r N + N_r \log[\det(\mathbf{R}_W)]. \quad (64)$$

REFERENCES

- [1] F. Liu, C. Masouros, A. P. Petropulu, H. Griffiths, and L. Hanzo, "Joint radar and communication design: Applications, state-of-the-art, and the road ahead," *IEEE Trans. Wireless Commun.*, vol. 68, no. 6, pp. 3834–3862, Jun. 2020.
- [2] E. C. Strinati *et al.*, "Wireless environment as a service enabled by reconfigurable intelligent surfaces: The RISE-6G perspective," in *Proc. Joint EuCNC/6G Summit*, Porto, Portugal, Jun. 2021, pp. 562–567.
- [3] N. C. Luong, X. Lu, D. T. Hoang, D. Niyato, and D. I. Kim, "Radio resource management in joint radar and communication: A comprehensive survey," *IEEE Commun. Surveys Tuts.*, vol. 23, no. 2, pp. 780–814, 2021.
- [4] J. A. Zhang *et al.*, "Enabling joint communication and radar sensing in mobile networks - a survey," *IEEE Commun. Surveys Tuts.*, vol. 24, no. 1, pp. 306–345, Oct. 2021.
- [5] H. Zhang *et al.*, "Holographic integrated sensing and communication," *IEEE J. Sel. Areas Commun.*, vol. 40, no. 7, pp. 2114–2130, Jul. 2022.
- [6] A. Babaei, W. H. Tranter, and T. Bose, "A nullspace-based precoder with subspace expansion for radar/communications coexistence," in *Proc. IEEE Glob. Commun. Conf. (GLOBECOM)*, Atlanta, GA, USA, Dec. 2013, pp. 3487–3492.
- [7] F. Liu, C. Masouros, A. Li, and T. Ratnarajah, "Robust MIMO beamforming for cellular and radar coexistence," *IEEE Wireless Commun. Lett.*, vol. 6, no. 3, pp. 374–377, Jun. 2017.
- [8] F. Liu, C. Masouros, A. Li, H. Sun, and L. Hanzo, "MU-MIMO communications with MIMO radar: From co-existence to joint transmission," *IEEE Trans. Wireless Commun.*, vol. 17, no. 4, pp. 2755–2770, Apr. 2018.
- [9] T. Tian, T. Zhang, L. Kong, and Y. Deng, "Transmit/Receive beamforming for MIMO-OFDM based dual-function radar and communication," *IEEE Trans. Veh. Technol.*, vol. 70, no. 5, pp. 4693–4708, May 2021.
- [10] Y. Liu, G. Liao, J. Xu, Z. Yang, and Y. Zhang, "Adaptive OFDM integrated radar and communications waveform design based on information theory," *IEEE Commun. Lett.*, vol. 21, no. 10, pp. 2174–2177, Oct. 2017.
- [11] K. Wu, J. A. Zhang, X. Huang, Y. J. Guo, and R. W. Heath, "Waveform design and accurate channel estimation for frequency-hopping MIMO radar-based communications," *IEEE Trans. Commun.*, vol. 69, no. 2, pp. 1244–1258, Feb. 2021.
- [12] M. Di Renzo *et al.*, "Smart radio environments empowered by reconfigurable intelligent surfaces: How it works, state of research, and the road ahead," *IEEE J. Sel. Areas Commun.*, vol. 38, no. 11, pp. 2450–2525, Nov. 2020.
- [13] Y. Liu *et al.*, "Reconfigurable intelligent surfaces: Principles and opportunities," *IEEE Commun. Surveys Tuts.*, vol. 23, no. 3, pp. 1546–1577, thirdquarter 2021.
- [14] C. Pan *et al.*, "An overview of signal processing techniques for RIS/IRS-aided wireless systems," *IEEE J. Sel. Topics Signal Process.*, vol. 16, no. 5, pp. 883–917, Aug. 2022.
- [15] C. Pan *et al.*, "Reconfigurable intelligent surfaces for 6G systems: Principles, applications, and research directions," *IEEE Commun. Mag.*, vol. 59, no. 6, pp. 14–20, Jun. 2021.
- [16] Q. Wu and R. Zhang, "Beamforming optimization for wireless network aided by intelligent reflecting surface with discrete phase shifts," *IEEE Trans. Commun.*, vol. 68, no. 3, pp. 1838–1851, Mar. 2020.
- [17] H. Guo, Y.-C. Liang, J. Chen, and E. G. Larsson, "Weighted sum-rate maximization for intelligent reflecting surface enhanced wireless networks," in *Proc. IEEE Glob. Commun. Conf. (GLOBECOM)*, Waikoloa, HI, United states, Dec. 2019, pp. 1–6.
- [18] X. Yu, D. Xu, and R. Schober, "MISO wireless communication systems via intelligent reflecting surfaces: (invited paper)," in *Proc. IEEE/CIC Int. Conf. Commun. China (ICCC)*, ChangChun, China, Aug. 2019, pp. 735–740.
- [19] G. Zhou, C. Pan, H. Ren, K. Wang, and A. Nallanathan, "A framework of robust transmission design for IRS-aided MISO communications with imperfect cascaded channels," *IEEE Trans. Signal Process.*, vol. 68, pp. 5092–5106, Aug. 2020.
- [20] X. Qian, M. Di Renzo, J. Liu, A. Kammoun and M. S. Alouini, "Beamforming through reconfigurable intelligent surfaces in single-user MIMO systems: SNR distribution and scaling laws in the presence of channel fading and phase noise," *IEEE Wireless Commun. Lett.*, vol. 10, no. 1, pp. 77–81, Jan. 2021.
- [21] Y.-C. Liang *et al.*, "Reconfigurable intelligent surfaces for smart wireless environments: channel estimation, system design and applications in 6G networks," *Sci. China Inf. Sci.*, vol. 64, no. 10, pp. 1–21, 2021.

- [22] T. L. Jensen *et al.*, “An optimal channel estimation scheme for intelligent reflecting surfaces based on a minimum variance unbiased estimator,” in *Proc. IEEE Int. Conf. on Acoust., Speech and Signal Process. (ICASSP)*, May 2020, pp. 5000–5004.
- [23] P. Wang *et al.*, “Compressed Channel Estimation for Intelligent Reflecting Surface-Assisted Millimeter Wave Systems,” *IEEE Signal Process. Lett.*, vol. 27, pp. 905–909, 2020.
- [24] J. He *et al.*, “Channel Estimation for RIS-Aided mmWave MIMO Systems via Atomic Norm Minimization,” *IEEE Trans. Wireless Commun.*, vol. 20, no. 9, pp. 5786–5797, Sep. 2021.
- [25] J. Mirza and B. Ali, “Channel Estimation Method and Phase Shift Design for Reconfigurable Intelligent Surface Assisted MIMO Networks,” *IEEE Trans. Cogn. Commun. Netw.*, vol. 7, no. 2, pp. 441–451, Jun. 2021.
- [26] L. Wei *et al.*, “Channel Estimation for RIS-Empowered Multi-User MISO Wireless Communications,” *IEEE Trans. Commun.*, vol. 69, no. 6, pp. 4144–4157, Jun. 2021.
- [27] H. Liu *et al.*, “Matrix-Calibration-Based Cascaded Channel Estimation for Reconfigurable Intelligent Surface Assisted Multiuser MIMO,” *IEEE J. Sel. Areas Commun.*, vol. 38, no. 11, pp. 2621–2636, Nov. 2020.
- [28] Y. Lin *et al.*, “Tensor-Based Algebraic Channel Estimation for Hybrid IRS-Assisted MIMO-OFDM,” *IEEE Trans. Wireless Commun.*, vol. 20, no. 6, pp. 3770–3784, Jun. 2021.
- [29] C. Liu *et al.*, “Deep residual learning for channel estimation in intelligent reflecting surface-assisted multi-user communications,” *IEEE Trans. Wireless Commun.*, vol. 21, no. 2, pp. 898–912, Feb. 2022.
- [30] A. Aubry, A. De Maio, and M. Rosamilia, “Reconfigurable intelligent surfaces for N-LOS radar surveillance,” *IEEE Trans. Veh. Technol.*, vol. 70, no. 10, pp. 10735–10749, Oct. 2021.
- [31] F. Wang, H. Li, and J. Fang, “Joint active and passive beamforming for IRS-assisted radar,” *IEEE Signal Process. Lett.*, vol. 29, pp. 349–353, Dec. 2022.
- [32] J. Hu *et al.*, “MetaSensing: Intelligent metasurface assisted RF 3D sensing by deep reinforcement learning,” *IEEE J. Sel. Areas Commun.*, vol. 39, no. 7, pp. 2182–2197, Jul. 2021.
- [33] X. Shao, C. You, W. Ma, X. Chen, and R. Zhang, “Target sensing with intelligent reflecting surface: Architecture and performance,” *IEEE J. Sel. Areas Commun.*, 2022, doi: 10.1109/JSAC.2022.3155546.
- [34] A. Elzanaty *et al.*, “Reconfigurable intelligent surfaces for localization: Position and orientation error bounds,” *IEEE Trans. Signal Process.*, vol. 69, pp. 5386–5402, 2021.
- [35] H. Zhang *et al.*, “Towards ubiquitous positioning by leveraging reconfigurable intelligent surface,” *IEEE Commun. Lett.*, vol. 25, no. 1, pp. 284–288, Jan. 2021.
- [36] E. Björnson *et al.*, “Reconfigurable Intelligent Surfaces: A Signal Processing Perspective With Wireless Applications,” *IEEE Signal Process. Mag.*, vol. 39, no. 2, pp. 135–158, Mar. 2022.
- [37] K. Keykhosravi *et al.*, “SISO RIS-Enabled Joint 3D Downlink Localization and Synchronization,” in *Proc. IEEE Int. Conf. Commun.*, Jun. 2021, pp. 1–6.
- [38] X. Wang, Z. Fei, J. Guo, Z. Zheng, and B. Li, “RIS-assisted spectrum sharing between MIMO radar and MU-MISO communication systems,” *IEEE Wireless Commun. Lett.*, vol. 10, no. 3, pp. 594–598, Mar. 2021.
- [39] Y. He, Y. Cai, H. Mao, and G. Yu, “RIS-assisted communication radar coexistence: Joint beamforming design and analysis,” *IEEE J. Sel. Areas Commun.*, 2022, doi: 10.1109/JSAC.2022.3155507.
- [40] R. S. Prasobh Sankar, B. Deepak, and S. P. Chepuri, “Joint communication and radar sensing with reconfigurable intelligent surfaces,” in *IEEE 22nd Int. Workshop Signal Process. Adv. Wireless Commun. (SPAWC)*, Piscataway, NJ, USA, Sep. 2021, pp. 471–475.
- [41] Z.-M. Jiang *et al.*, “Intelligent reflecting surface aided dual-function radar and communication system,” *IEEE Syst. J.*, vol. 16, no. 1, pp. 475–486, Feb. 2021.
- [42] X. Wang, Z. Fei, Z. Zheng, and J. Guo, “Joint waveform design and passive beamforming for RIS-assisted dual-functional radar-communication system,” *IEEE Trans. Veh. Technol.*, vol. 70, no. 5, pp. 5131–5136, May 2021.
- [43] X. Liu *et al.*, “Proximal policy optimization-based transmit beamforming and phase-shift design in an IRS-aided ISAC system for the THz band,” *IEEE J. Sel. Areas Commun.*, 2022, doi: 10.1109/JSAC.2022.3158696.
- [44] F. Liu and C. Masouros, “A tutorial on joint radar and communication transmission for vehicular networks—part III: Predictive beamforming without state models,” *IEEE Commun. Lett.*, vol. 25, no. 2, pp. 332–336, Feb. 2021.
- [45] B. Tang, J. Tang, and Y. Peng, “MIMO radar waveform design in colored noise based on information theory,” *IEEE Trans. Signal Process.*, vol. 58, no. 9, pp. 4684–4697, Sep. 2010.

- [46] Y. Xu, Y. Li and J. Wu, "Weighted sum-rate outage probability constrained transmission design for IRS-enhanced communication," in *Proc. IEEE Wireless Commun. Networking Conf. (WCNC)*, Austin, TX, United states, Apr. 2022, pp. 1081-1086.
- [47] J. Nocedal and S. J. Wright, *Numerical Optimization*. NewYork, NY, USA: Springer, 2006.
- [48] S. Boyd and L. Vandenberghe, *Convex Optimization*. Cambridge, U.K.: Cambridge Univ. Press, 2004.
- [49] Z. Luo, W. Ma, A. M. So, Y. Ye, and S. Zhang, "Semidefinite relaxation of quadratic optimization problems," *IEEE Signal Process. Mag.*, vol. 27, no. 3, pp. 20–34, 2010.
- [50] Q. Wu, Y. Zeng, and R. Zhang, "Joint trajectory and communication design for multi-UAV enabled wireless networks," *IEEE Trans. Wireless Commun.*, vol. 17, no. 3, pp. 2109–2121, Mar. 2018.